On Optimization of Some Parameters in Ultrasonic Metal Welding

Understanding of the weld forming process leads to a way of optimizing some parameters in ultrasonic welding

BY U. I. CHANG AND J. FRISCH

ABSTRACT. The fundamental bonding mechanisms of ultrasonic welding are discussed and two basic bond forming processes are suggested. An optimum weld condition for the electric power inputs was formulated using elastic and plastic analysis and a semianalytic expression for the optimum electric power input was thus obtained. The validity of the expression was checked by a series of experiments with 2024-T351 aluminum and OFHC copper. An expression for the coefficient of friction for alternating tangential motion was also obtained from this analysis. The strength characteristics of the welds are compared for different test conditions and failure modes.

Introduction

Ultrasonic welding is a method of joining similar or dissimilar metals by applying high frequency shear vibration and normal pressure to the weld interface. The mechanical energy transmitted to the weld area produces a sound metallurgical bond between two metals. The major advantage of this welding technique over conventional fusion joining processes is low heat input at the weld. Thin

Nomenclature

- A Tangential displacement of the sonotrode tip vibration 10^{-3} in.
- A_{op} Optimum tangential displacement of the sonotrode tip vibration, 10^{-3} in.
- a Radius of the contact area, in.
- b Radius of the inner boundary of a slip annulus, in.
- d Diameter of a sphere, or diameter of the disk specimen, in.
- E Young's modulus, psi
- k Constant
- G Shear modulus, psi
- N Normal load or weld clamping force, lb
- P Electric power input to the transducer, watts
- P_{op} Optimum electric power input, watts
- p Normal stress at the contact area, psi
- p_{max} Maximum normal stress at the contact area, psi $P_{max} = 3/N2\ \pi\ a^2$
- S Tangential shear force, lb
- t Ultrasonic pulse time or weld time, sec
- X_s Minimum sonotrode tip displacement required for a fully developed slip annulus, 10^{-3} in.
- X_p Maximum allowable displacement for sublayer plastic deformation when an optimum weld is produced, 10^{-3} in.
- X A small sonotrode tip displacement by which a slip annulus is produced, 10^{-3} in.
- ν Poisson's ratio, dimensionless
- τ_y Shear yield stress, psi
- τ Shear stress, psi
- γ Maximum allowable shear strain for sublayer plastic deformation at the weld, %
- μ Coefficient of friction when an oscillating tangential vibration is applied to the contact between an elastic sphere and an elastic flat, dimensionless

U. I. CHANG is associated with the Welding Development Department, Manufacturing Development Office of the Ford Motor Company. J. FRISCH is Professor of Mechanical Engineering, University of California, Berkeley, California.

Paper was presented at the 54th AWS Annual Meeting held in Chicago during April 2-6, 1973

foils or wires can be welded to thick members and the unfavorable changes in material properties due to heat at or around the weld are less significant. Also, shrinkage and distortion problems are absent from this welding technique. This joining process is utilized in spot-type welding, ring welding, line welding, and continuous-seam welding (Ref. 1).

For spot-type welding, the variables under control of the welding machine operator are tip radius, normal load, electric power input to the transducer and weld time. Proper adjustment of these variables is essential to minimize the required energy and optimize weld quality for any material combination. The vibratory frequency, which may range from 10,000 to 175,000 Hz, is determined by the welding machine design and is not believed to be critical (Ref. 1) in ultrasonic welding.

The basic mechanism by which ultrasonic welds are produced is believed to be solid-state bonding (Refs. 1-7). Static normal pressure and oscillating shear stresses at the weld interface result in localized slip at the weld interface and plastic deformation in a thin sublayer enveloping the interface. This process breaks up contaminant films and produces an area of metal-to-metal contact. Even though this joining technique is widely used in industry, the basic theory for this welding process is not completely understood because of the complexity involved in the formation of welds. Good welding practice often relies on a trial and error method even though some variables have an experimental equation for guidance.

The objective of this study is to develop clearer understanding of the bonding mechanism and processes, and to formulate an expression of variables for the optimum welding conditions. In order to eliminate the complexity involved in a multi-interface problem found in commercial ultrasonic welding, the sonotrode tip in a conventional welding system was, for experimental purposes, replaced by a disk specimen with a spherical radius as shown in Fig. 1. This disk specimen was ultrasonically welded to a flat block specimen which was tightly fixed to a massive anvil. Such a configuration enabled direct application of vibratory energy to the weld interface, and simplified the analysis of weld formation.

Mechanism of Ultrasonic Welding

Ultrasonic welding of metals consists of interrelated, complex processes such as plastic deformation, work-hardening, breaking of contaminant films, fatigue, crack formation and propagation, fracture, generation of heat by friction and plastic deformation, recrystallization, and interdiffusion. Although the generally accepted mechanism is solid state bonding some investigators have suggested that ultrasonic welding is another form of fusion welding activated by the heat generated through friction and plastic deformation, or at least it is a strongly heat-assisted welding process (Refs. 8-11).

The localized temperature rise at the weld in ultrasonic welding is due to the combined effect of elastic hysteresis, localized interfacial slip, and plastic deformation. Temperature measurements made with materials covering a wide range of melting temperatures show that the maximum average interface temperature when good welds are produced ranges from 35 to 50% of the absolute melting temperature of the material, suggesting no melting in the weld zone (Ref. 1). These observations strongly support the solid state bonding mechanism.

Adhesion, one of the solid state bonding mechanisms, requires an intimate contact of the interface. The presence of surface films is detrimental to achieve atomically close contact of two metal surfaces. Surface films, especially oxide films, should either be removed or broken in such a way that clean metals be in contact. Bond strength then depends upon the areas where metal-to-metal contact is achieved. In ultrasonic welding of metals, the breaking of contaminant films for intimate metal-to-metal contact is accomplished by the combined alternating shear stresses at or around the weld, which result from the normal load and oscillating tangential force.

The relative tangential displacement between a pair of contacting bodies can cause localized interfacial slip and sublayer plastic deformation around the interface if no gross sliding is assumed. Here "sliding" refers to the uniform movement or displacement of one contacting surface over another while "slip" is used for localized tangential displacement at the contacting surface. Gross sliding can occur when the relative displacement is large enough or the frictional force is small enough to slide.

In ultrasonic welding, both localized slip and sublayer plastic deformation are desirable. The interfacial slip breaks up surface films allowing metal-to-metal contact at higher asperities and subsequently a large number of small bonded areas are formed over the entire contacting area (Ref. 4).

The plastic deformation in the sublayer enveloping the interface can occur when the relative displacement is larger than that necessary to cause slip and the frictional stress is higher than the flow stress of sublayer material. If the frictional stress is lower than the flow stress, gross sliding will occur. Defining μ as the coefficient of friction when an oscillating tangential force is applied to the weld, plastic deformation starts when the following condition is met:

$$\mu N = k\,(\text{area})\ \ \tau_y = k\,(\pi a^2)\ \ \tau_y \qquad (1)$$

This plastic deformation causes further breakup of the contaminant films, and displacement of broken particles in the vicinity of the interface in a random manner. Figure 2 illustrates this process.

The oscillating plastic shear can induce metal circulation across the interface and produce a severely work hardened weld, which sometimes self anneals to a very fine grain structure. This phenomena has been observed in 2024-T351 aluminum welds (Ref. 1). Plastic deformation in the sublayer is the primary process

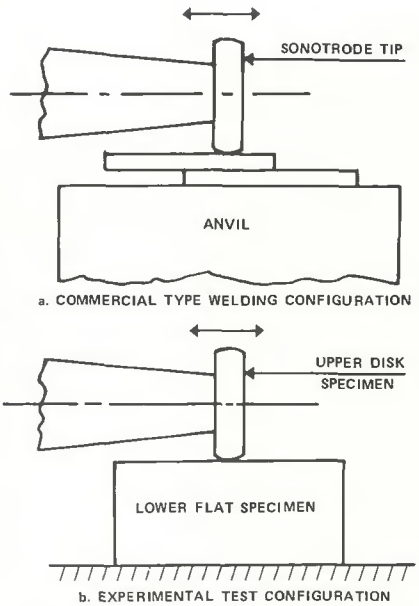

Fig. 1 — Ultrasonic welding configurations

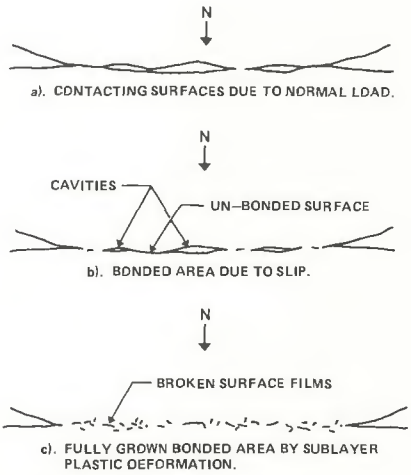

Fig. 2 — Evolution of bonded area due to ultrasonic vibration

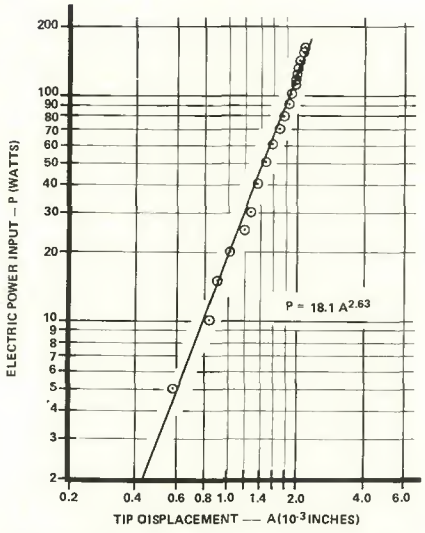

Fig. 3 — Electrical power vs. displacement of the sonotrode tip vibration for the ultrasonic welding system

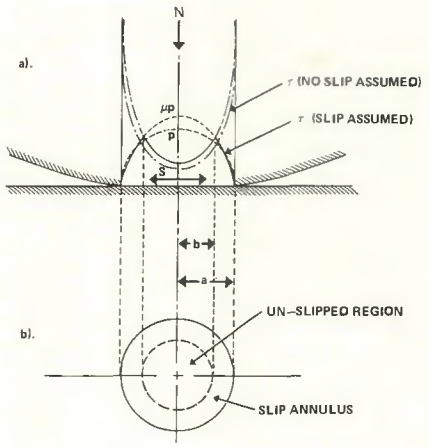

Fig. 4 — (a) Distribution of normal stress and shear stress over contact area between an elastic sphere and an elastic flat with normal load N and tangential force S. (b) slip annulus

for high bond strength. The most plausible bonding mechanism during the plastic deformation stage is solid state bonding such as adhesion, mechanical interlocking of the surfaces, recrystallization, and diffusion.

In summary, the dominating mechanism for ultrasonic welding is solid state bonding, and it is accomplished by two different processes: slip and plastic deformation. The bond formation is mainly attributed to the latter stage.

Weld Strength and Welding Variables

Weld strength is the breaking load necessary to separate the weld, and if the weld is separated by a force acting normal to the weld interface, this breaking load is known as tensile weld strength. If separation results from a shear force acting parallel to the weld interface, one speaks of shear weld strength. It is known that weld strength is deteriorated by excessive power during ultrasonic welding. This is attributed to fatigue cracks developed at the interface (Refs. 4, 5, 12) or excessive damage of the weldment by overstressing (Ref. 13). Many investigators found cracking occurred in ultrasonic welds (Refs. 3, 4, 9, 10). An optimum ultrasonic weld can be made when sufficient plastic deformation occurs without serious weld deterioration by fatigue cracking or overstressing.

The weld strength in spot-type welding is affected by the setting of such variables as tip radius, normal load, electric power input and weld time. Since a larger tip radius increases the weld area, other variables are adjusted to allow proper plastic deformation of the weld. The normal load, combined with the tangential force, should be high enough to plastically deform the sublayer, a condition imposed by Eq. 1. The normal load range varies with power capacity of the machine, and desirable normal loads for any specific welding application depend on the thickness and hardness of the components (Ref. 1).

Energy requirements to produce a good weld vary with the properties and thickness of materials being welded. Insufficient power usually results in low weld strengths due to insufficiently grown bonded area; however, excessive high power deteriorates the weld integrity by either introducing cracks or shearing the already formed weld. The degree of plastic deformation at the weld is determined by the electric power input and the weld strength will be optimum for a specific value of electric power input when other variables remain constant. The electric power input is generally related to the vibrational displacement of the sonotrode tip as shown in Fig. 3. Once this relationship is found for a particular welding system, the conversion of power to tip displacement is possible. The sonotrode tip displacement is more meaningful than electric power input delivered to the transducer in analyzing plastic deformation at the weld. The optimum tip displacements are those which allow optimum weld strengths when other variables are constant.

The effect of weld time on weld strength is important since prolonged weld times result in fatigue damage (Ref. 4), and insufficient weld times show incomplete welds. The minimum time required appears to vary with the thickness of the workpiece which is in contact with sonotrode tips. Practical range is about 0.005 sec for very fine wires to about 1.2 sec for heavier materials (Ref. 1).

Optimum Sonotrode Tip Displacement

If an elastic sphere is pressed against an elastic flat with a normal load N, the normal stress distribution over the contact surface p can be represented (Ref. 14) by the ordinates of a hemisphere of radius "a" constructed on the surface of contact as shown in Fig. 4. If "a" is the radius of the circular contact surface, the normal stress p at any distance r is given by

$$p = p_{max}\left\{1 - \left(\frac{r}{a}\right)^2\right\}^{1/2} \qquad (2)$$

Mindlin (Ref. 15) studied the effects of an oscillating tangential force on the contact surface of two elastic spheres. The assumption that slip cannot occur at any part of the contact surface is untenable because it required the shear stress rising to infinity at the boundary of contact as shown in Fig. 4. Hence, slip was expected to begin at the boundary and progress inward with increasing tangential shear force S , under the assumption that shear stress cannot exceed the product of constant coefficient of friction and normal stress given by Eq. 2. As shown in Fig. 4, this slip region has an annular shape called slip annulus. The surface is plastically deformed by slip and the original surface topography is damaged (Ref. 16).

The slip annulus grows with increased value of S as can be seen from the following equation by Mindlin (Ref. 15).

$$b = a\left(1 - \frac{S}{\mu N}\right)^{1/3} \qquad (3)$$

The slip annulus starts along the boundary of contact area and grows inwards until it covers the whole area of contact as S varies from O to μ N; i.e., S/μN varies from 0 to 1. Mindlin obtained another equation, valid until the contact surfaces start to slide over each other, which relates the shear force S to the tangential displacement X of the top sphere.

$$X = \frac{3(2-\nu)}{8Ga}\mu N\left\{1 - \left(1 - \frac{S}{\mu N}\right)^{2/3}\right\} \qquad (4)$$

Combining Eqs. 3 and 4, it can be seen that the slip annulus grows with increasing tangential displacement X, as shown in Eq. 3-a.

$$b = a\left\{1 - \frac{8Ga}{3(2-\nu)\mu N}X\right\}^{1/2} \qquad (3\text{-a})$$

Mindlin assumed that the two spheres had the same radius and the same elastic properties; however, his results were not seriously affected by the radii of the spheres for a given size of contact area (Ref. 5). Substi-

tuting Eq. 3 into Eq. 4 gives the following expression:

$$X = \frac{3(2-\nu)}{8Ga}\mu N \left\{1-\left(\frac{b}{a}\right)^2\right\} \quad (5)$$

Therefore, the tip displacement for a fully developed slip annulus X_s is

$$X_s = \frac{3(2-\nu)}{8Ga}\mu N \quad (6)$$

This equation can also be obtained by substituting the condition $S/(\mu N) = 1$ into Eq. 4.
From Eqs. 5 and 6,

$$X_s = \frac{X}{1-(b/a)^2} \quad (7)$$

This expression predicts the tip displacement X_s required to have a fully developed slip annulus without knowledge of the value of μ.

The ratio b/a can be directly measured from the damaged slip annulus produced by tangential vibration with a small tip displacement. If the tip displacement is larger than X_s, either sliding at the interface or plastic deformation at the sublayer can occur. Sliding at the interface will occur if μN is lower than the tangential force needed to plastically deform the sublayer. If μN is higher than that, the sublayer will plastically deform, and excessive displacement will be accommodated by sublayer plastic deformation.

Since both maximum slip area at the contact surface and proper degree of plastic deformation in the sublayer are desirable for the optimum weld strength, the optimum tip displacement A_{op} will have the expression

$$A_{op} = X_s + X_p \quad (8)$$

where X_p is the plastic displacement of the sublayer. As tip displacement increases, different bonding processes predominate as shown in Fig. 5. Also shown is the theoretical tangential force and the expected tensile weld strength as a function of tip displacement. Appreciable bond strength starts to form at X_s, and the maximum occurs at A_{op}. The decreasing slope of tensile weld strength after A_{op} depends on the susceptibility of the material to fatigue or overstressing.

The stress distributions at the contact area and along the center line joining the centers of spheres are known for the case of two elastic spheres pressed together (Refs. 14, 17). According to the analysis (Ref. 14), the maximum shear stress is developed on the center line at a depth of about one half the radius of the contact area. The magnitude is about 0.31 p_{max} for $\nu = 0.3$ where p_{max} is the maximum pressure developed at the contact area. This point is where the plastic deformation can start first by additional tangential shear stresses.

The theoretical plastic zone at the interface has a lenticular shape with center thickness a and diameter 2a as shown in Fig. 6. This may be approximated by a disk with a uniform thickness a/2 and a diameter of 2a. The lenticular shape of the plastic zone is proved by a weld bead (Ref. 18) produced at the weld interface of 17-4 PH stainless steel as shown in Fig 6-c. Since the radius of contact area is, as given by Hertz (Ref. 19),

$$a = 0.88 \sqrt[3]{(Nd/E)} \quad (9)$$

the uniform thickness of the plastic layer t_p can be assumed as

$$t_p \approx a/2 = 0.44 \sqrt[3]{(Nd/E)} \quad (10)$$

for a sphere and a flat contact. If we further assume that this disk with uniform thickness t_p has uniform plastic deformation by shear, the maximum allowable plastic displacement by this layer X_p can be expressed as

$$X_p = a\gamma/2 = 0.44\,\gamma\sqrt[3]{(Nd/E)} \quad (11)$$

where γ is the maximum allowable shear strain of the sublayer without deteriorating the weld integrity by either fatigue cracking or overstressing.
Now, the expression for the optimum tip displacement A_{op} is,

$$A_{op} = X_s + X_p = \frac{X}{1-(b/a)^2} + 0.44\,\gamma\sqrt[3]{(Nd/E)} \quad (12)$$

Another interesting equation is the expression of μ obtained by substituting Eq. 9, shear modulus
$G = E/2(1+\nu)$ and $\nu = 0.3$ into Eq. 6.

$$\mu = 0.53\,(E^2 d/N^2)^{1/3} X_s \quad (13)$$

Experimental Equipment

The experimental equipments, shown in Fig. 7, consist of the vacuum apparatus, loading and measuring devices, and ultrasonic instrumentation. Pumping in the low vacuum region was accomplished by a mechanical pump of 10 cubic feet/minute capacity, or two double Varian VacSorb pumps, as shown in Fig. 7. High vacuum pumping was performed by a 75 liter/sec ion pump. A standard thermocouple vacuum gauge was used during rough pumping and a Bayard-Alpert type nude ionization gage and a partial pressure

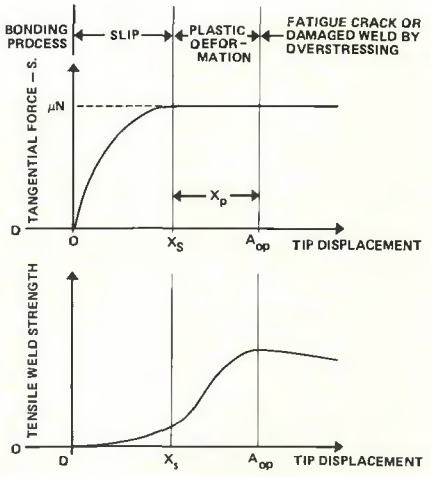

Fig. 5 — Variation of bonding process and expected tensile weld strength

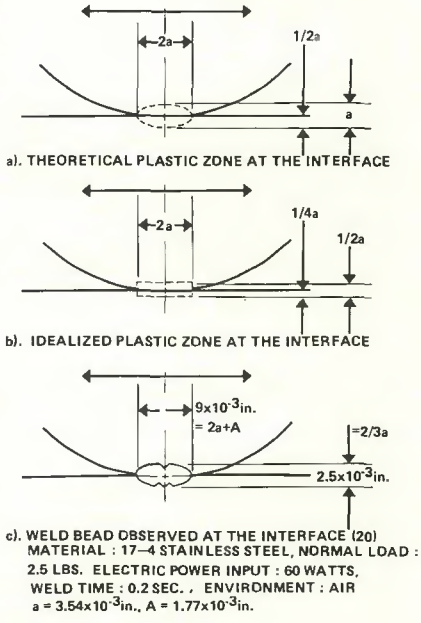

Fig. 6 — Plastic zone at the interface

gage (PPG) monitored the system pressure in the high vacuum range. The seal for linear motion and linear-rotational motion through the vacuum chamber was provided by stainless steel bellows.

The compressive and tensile loads were supplied by a lever system installed outside of the chamber. The normal load strain gage dynamometer was a 4-arm bending beam to minimize anvil rotation. The anvil with specimen clamp was attached to the ends of the 4 arms as shown in Fig. 8. Four strain gages formed a bridge circuit to measure the compressive normal load N on the specimens during welding and the tensile force required to separate the specimens after welding. The minimum sensitivity of the dynamometer was

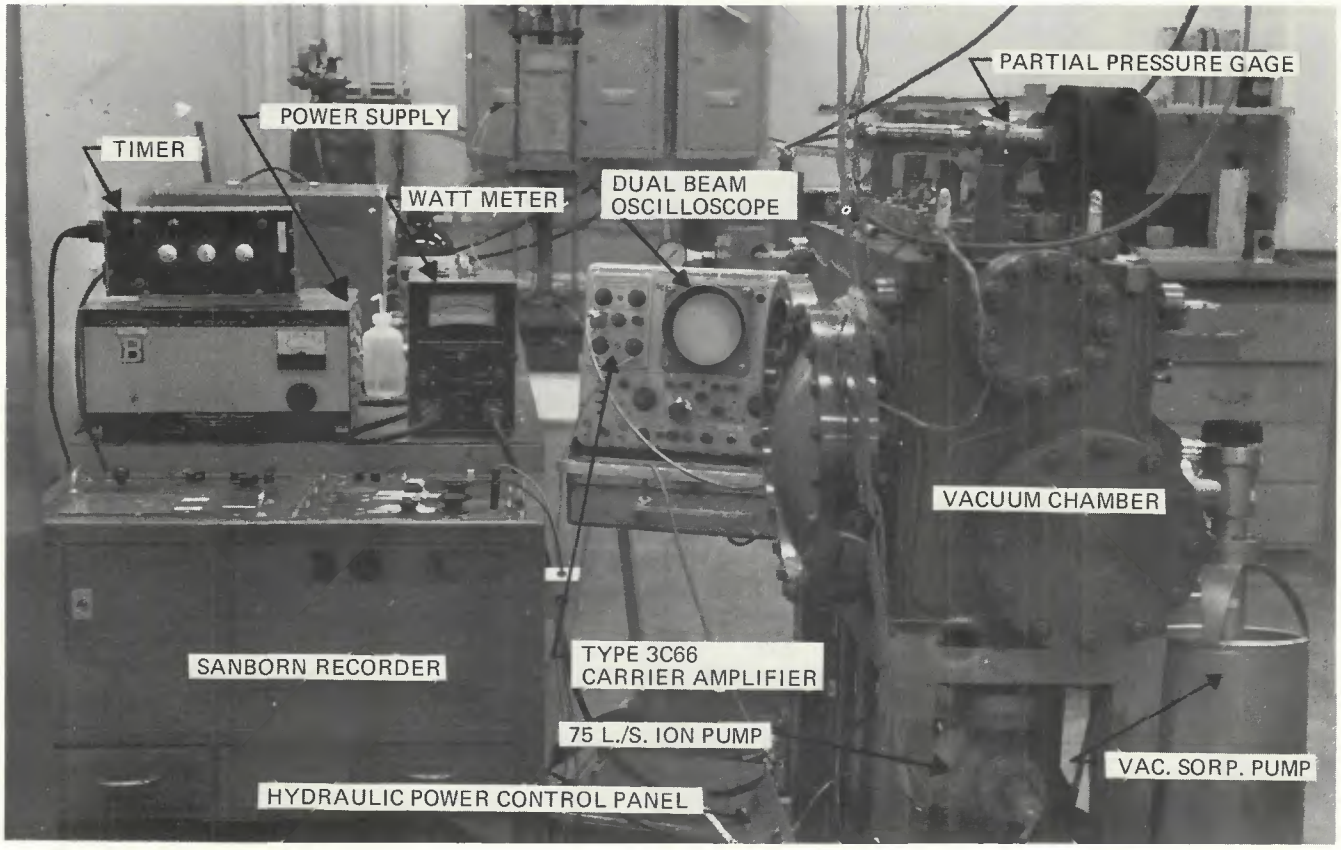

Fig. 7 — Experimental apparatus

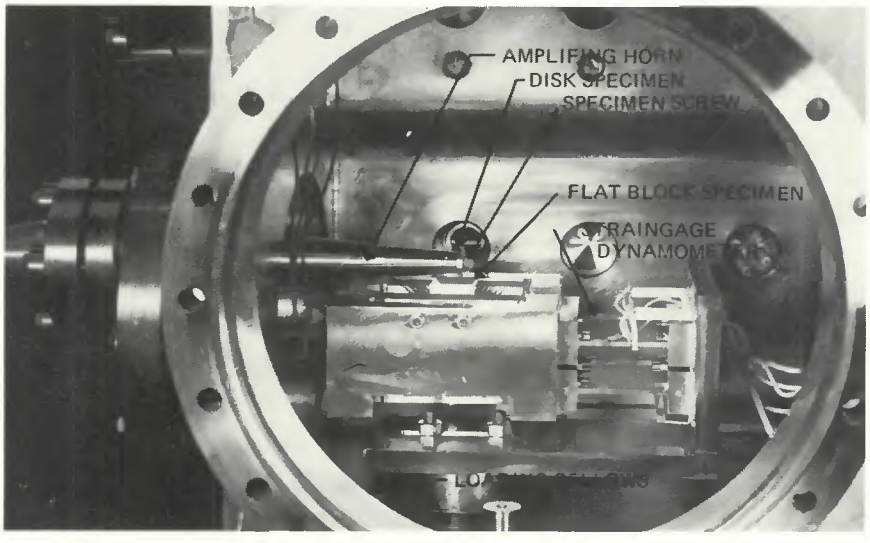

Fig. 8 — Specimen test assembly for tensile weld strength test

0.1 lb and the maximum allowable load was 135 lb (Ref. 19). Figure 8 shows the installed dynamometer and anvil assembly with specimens in position.

To investigate the shear strength characteristics of the ultrasonically welded joints, a different loading and unloading system was used. This loading system is composed of an anvil, normal load and a torque dynamometer, a torque box with three stainless steel bellows, and a hydraulic load applying system (Ref. 18). This mechanism enabled the anvil to have linear vertical motion of 1 in. and independently 45 deg rotational motion with excellent vacuum sealing. Both dynamometers were placed inside the vacuum chamber close to the anvil for more accurate measurements. Each dynamometer has four strain gages to form a bridge circuit. The normal load dynamometer was designed for a range from 0.2 to 200 lb and torque dynamometer for a range from 0.2 to 200 lb in.

The ultrasonic system, a schematic block diagram of which is shown in Fig. 9, was used to generate high intensity ultrasonic vibrations at the specimen interface. The ultrasonic pulse length was controlled by a electronic decade interval timer, and the 150 watt J-17* power supply incorporated with an automatic frequency control was used. Power was recorded with a WAJ2* watt meter. The 20 kHz output of the power supply was then fed into an ultrasonic transducer, which utilized a lead titanate zirconate crystal to convert the electrical output of the power supply into longitudinal mechanical vibrations with a 20 kHz frequency. The coupling horn attached to the transducer provided a convenient location at which the vacuum feed-through could be made. For this particular study, an exponential amplifying horn was selected (Ref. 20), and the particular dimensions yielded an amplification ratio of approximately 3. A typical transducer displacement for full power operation was 0.0007 in., yielding a displacement of approximately 0.002 in. at the tip of an exponential amplifying horn.

*Branson Sonic Power Co.

Experimental Technique

For the two materials used in this investigation, the specimens shown in Fig. 10 were made from 1 in. bar stock of 2024-T351 aluminum alloy and 1 in. OFHC copper plate. The surface finish was 8 micro in. RMS and acetone was used for degreasing before each test.

The disk specimen was attached to the tip of the amplifying horn and the block specimen was clamped in the anvil of the dynamometer block, as shown in Fig. 8. The dynamometer assembly was then raised for contact between the disk and block specimen. Since the disk specimen was the central portion of a 3/4 in. diam sphere and the block specimen had a flat surface, they modeled a sphere on flat contact configuration. The timer shown in Fig. 7 controlled the ultrasonic pulse durations of 0.2 and 1.0 sec used in the experiments. As a relative measure of the ultrasonic power at the tip of the amplifying horn, the electrical power input P to the ultrasonic transducer was recorded with a watt meter.

The tensile weld strengths were measured for experiments of various electric power input levels with preset normal contacting loads and ultrasonic pulse durations. Usually a series of tests was done at different locations of one disk and one block specimen to minimize variations in parameters such as surface roughness and cleanliness. The same test procedure was used in the atmospheric environment as well as a vacuum environment in the range of 2×10^{-7} to 4×10^{-7} torr**

The shear strength tests for ultrasonically welded OFHC copper were done in the previously described apparatus (Ref. 21). The disk specimen was again attached to the amplifying horn tip and the block specimen was mounted in an anvil. Contact of the two specimens was 1.57 in. from the center of anvil rotation in order to provide a torque arm for the shear force acting at the weld when two specimens were separated. This offset was large enough compared to the weld area so that transverse shear instead of torsional shear occurred at the weld. The entire anvil assembly was raised hydraulically and the normal compressive load during contact was monitored with the normal load dynamometer. Normal load was maintained constant during welding and reduced to zero for shear tests. A normal load of 20 lb and a 1.0 sec weld time were used in the shear test series for both OFHC copper and 2024-T351 aluminum. Tests were done both in air and vacuum from 5×10^{-5} to 7×10^{-6} torr, with an electric power input up to 140 watts.

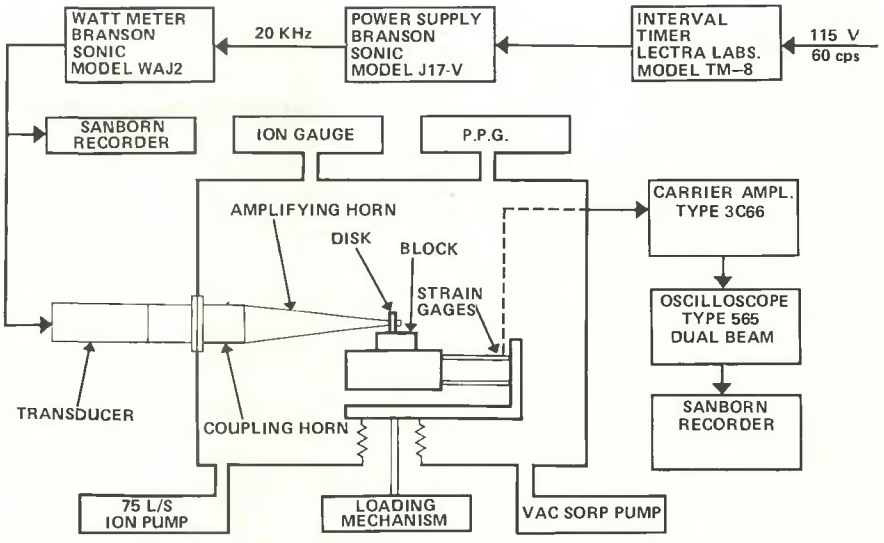

Fig. 9 — Schematic diagram of ultrasonic welding system for tensile weld strength tests

To find the relationship between electrical power input and the amplitude of the ultrasonic vibration of the disk specimen, one edge of the aluminum disk specimen on the horn tip was ground flat and polished. Movement of the square edge of the flat surface was observed with an ordinary microscope with a graduated eyepiece. The ultrasonic vibration of the specimen extended the image of the edge to a value of one amplitude. By measuring these extended regions of the specimen image, the following relationship was obtained for the experimental configuration of this ultrasonic welding investigation.

$$P = 18.1\, A^{2.63} \qquad (14)$$

where A is the sonotrode tip displacement and P the electric power input to the transducer. Experimental data are shown in Fig. 3. The original data were obtained with a free disk specimen; i.e., the disk specimen was not in contact with the block specimen. However, five data points were checked with the same disk specimen in contact with an aluminum block specimen. Electric power input of 10, 30, 60, 90, and 120 W with 30 lb normal load did not give any appreciable change in vibration amplitudes compared to those of free vibration.

It was also found that the block specimen did not follow the vibration while it was being ultrasonically welded with a 30 lb normal load and 120 W electric power input. Since no detectable amplitude of vibration was observed at one edge of the block specimen, the tip displacement shown in Fig. 3 can be considered as the relative displacement between two specimens while they were ultrasonically welded. From Eqs. 14 and 12, an expression for optimum electric power input is obtained for this ultrasonic welding investigation.

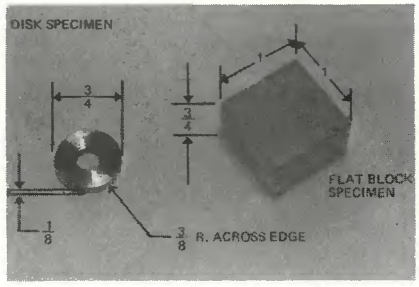

Fig. 10 — Ultrasonic welding specimens

$$P_{op} = 18.1 \left[\frac{X}{1-(b/a)^2} + 0.44\, \gamma \sqrt[3]{(Nd/E)} \right]^{2.63} \qquad (15)$$

Experimental Results and Discussions

A series of tensile weld strength curves was obtained for 2024-T351 aluminum when normal loads of 2.5, 5, 10, 20, and 30 lb were applied and 0.2 and 1.0 sec weld times were used. For each combination of test conditions, the electric power input was varied up to 120 W or occasionally to 140 W. The measured tensile strengths of the welds are plotted as a function of electric power input. Each tensile strength curve has an optimum value which varies according to applied normal load and weld time, as shown in Fig. 11. Higher normal loads required higher electric power inputs for the optimum weld and the 1.0 sec weld time series showed somewhat lower values of the optimum electric power input than the 0.2 sec weld time series. These opti-

** *1 torr = 1 mm Hg*

Table 1 — Calculated and Observed Values of Optimum Sonotrode Tip Displacement for 2024-T351 Al Welding, in Air

N, lb	t, sec	Power, w	Ampl., 10^{-3} in.	b/a	X_s cal., 10^{-3} in.	X_s obs., 10^{-3} in.	a/2 10^{-2} in.(a)	X_p cal., 10^{-3} in.(b)	A_{op} cal., 10^{-3} in.	P_{op} obs., W	A_{op} obs., 10^{-3} in.
30	1	15	0.94	0.568	1.38	>1.21	0.566	0.510	1.89	90	1.84
30	0.2	15	0.94	0.54	1.32	>1.21	0.566	0.510	1.83	105	1.93
20	1	15	0.94	0.316	1.05	<1.21	0.494	0.445	1.50	45	1.41
20	0.2	—	—	—	—	—	—	—	—	60	1.58
10	1	8	0.73	0.52	1.00	<1.21 >0.94	0.392	0.353	1.35	30	1.20
10	0.2	—	—	—	—	—	—	—	—	45	1.40
5	1	4	0.57	0.48	0.74	—	0.311	0.279	1.02	15	0.94
5	0.2	—	—	—	—	—	—	—	—	30	1.20
2.5	1	4	0.57	1.00	0.57	—	0.247	0.222	0.79	15	0.94
2.5	0.2	—	—	—	—	—	—	—	—	30	1.20

(a) Material Properties of 2024-T351 aluminum (Ref. 22): $E = 10.6 \times 10^6$ psi., elongation (in 2 in., 1/2 in. diam specimen) = 19% (typical).
(b) γ = 9% was used for calculation.

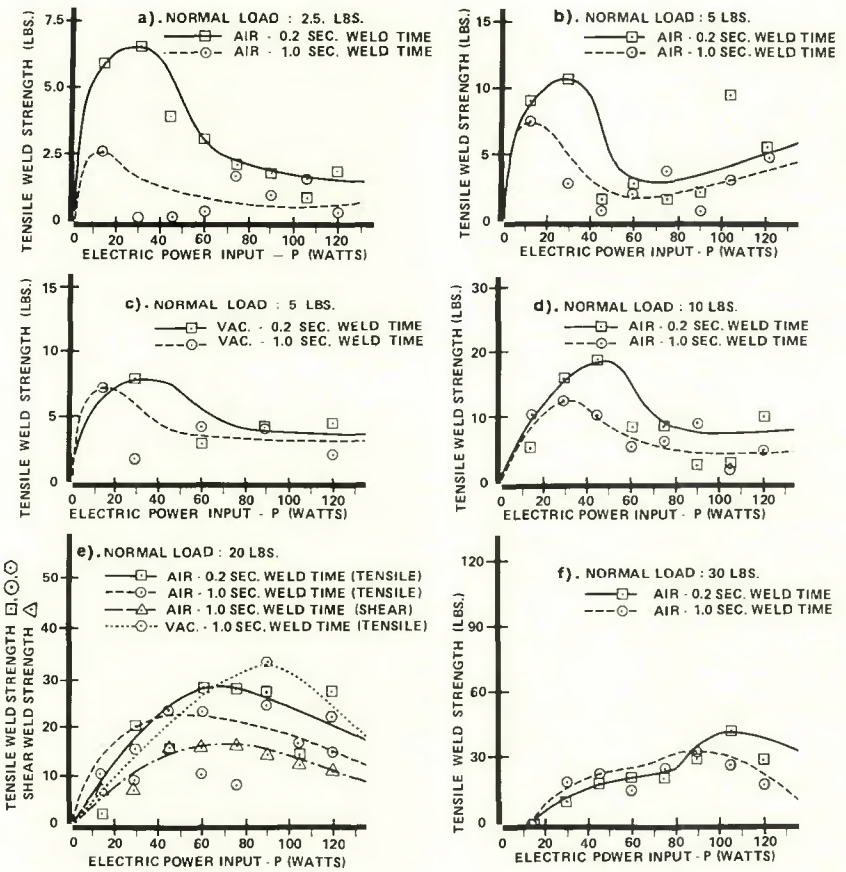

Fig. 11 — Tensile weld strength or shear weld strength vs. electric power input for 2024-T351 aluminum

mum weld strengths, plotted as functions of normal load, are shown in Fig. 12. Curves of optimum electric power input versus normal load are shown in Fig. 13 which shows that the optimum normal load increases with increased electric power input. These power values have been converted to corresponding tip displacements of the disk specimen by using the relationship shown in Fig. 3, and these optimum tip displacements, as functions of normal load, are shown in Fig. 14.

Experiments were performed to obtain slip annuli for different normal loads. To produce such slip annuli, electric power inputs ranging from 4 to 15 W, which correspond to tip displacements of 0.57×10 to 0.94×10^{-3} in., were applied. The b/a ratios of the slip annuli were measured from the broken welds with a microscope and the values of X_s were calculated using Eq. 7. Calculated values are listed in Table 1 and agree with the observed values of X_s. Some of the slip annuli are shown in Fig. 15. For comparison, fully developed slip annuli made under different normal load or power input are shown in Fig. 16.

Calculations for the plastic displacement X_p require a value for the allowable shear strain at the weld γ. In general, ductile materials should have higher γ than brittle materials. The analytical prediction of γ is difficult, if possible, because of high strain rates involved in a high frequency vibration, temperature rise, fatigue problems, size effect at the weld, and geometric constraint imposed by surrounding material. Therefore, this value has been obtained from one set of data (N = 30 lb) and is then used for the rest of the calculations. The computed value of γ was found to be equal to approximately one-half the typical tensile elongation (Ref. 22). One half of the radius of contact area was calculated for different normal loads and then multiplied by a constant value of γ to obtain X_p. The optimum tip displacement A_{op} was obtained by adding X_p to X_s as shown in Table 1. The calculated values of A_{op}'s are plotted in Fig. 14 for comparison with observed data.

Equation 12 was also used to calculate A_{op} for OFHC copper welding. Observed optimum power inputs for OFHC copper with 5 lb normal load were 25 W for 1.0 sec weld time and 35 W for 0.2 sec weld time (Ref. 19). A calculated value of A_{op} from Eq. 12 gave 1.05×10^{-3} in. for the optimum tip displacement. Again, the value of γ was taken as one-half of the reported elongation value (Ref. 23). Calculations are listed in Table 2.

Table 2 — Calculated and Observed Values of Optimum Sonotrode Tip Displacement for OFHC Copper Welding in Air

N, lbs	Power, W	Ampl., 10^{-3} in.	b/a	X_s cal., 10^{-3} in.	a/2 10^{-2} in.(a)	X_p cal., 10^{-3} in.(b)	A_{op} cal., 10^{-3} in.	t, sec	A_{op} obs., W	A_{op} obs., 10^{-3} in.
5	2	0.47	0.316	0.52	0.266	0.53	1.05	0.2	35	1.10
								1.0	25	0.97
20	8	0.73	1.00	0.73	0.422	0.844	1.57	1.0	60	1.58

(a) For OFHC copper (Ref. 23): E = 17 × 10^6 psi.; elongation (in 2 in.) = 45 to 35%.
(b) γ = 20% was used.

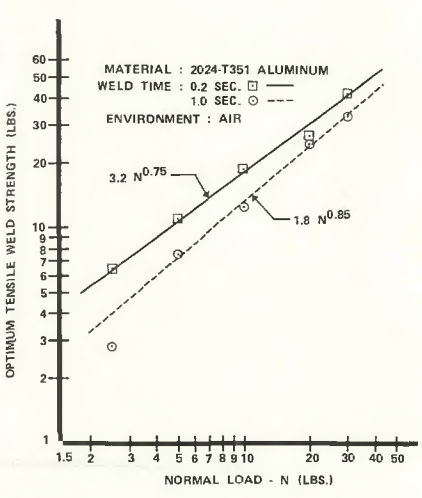

Fig. 12 — Optimum tensile weld strength as a function of normal load for 2024-T351 aluminum in air

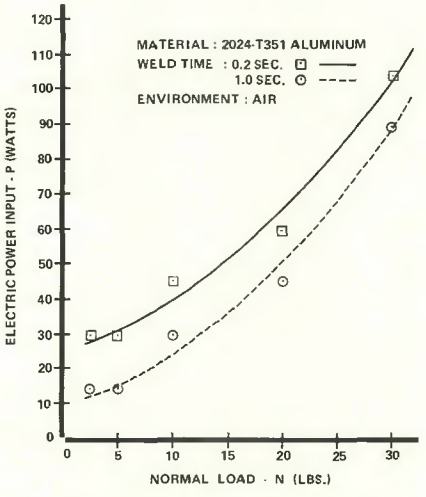

Fig. 13 — Optimum power as a function of normal load in tensile weld strength tests

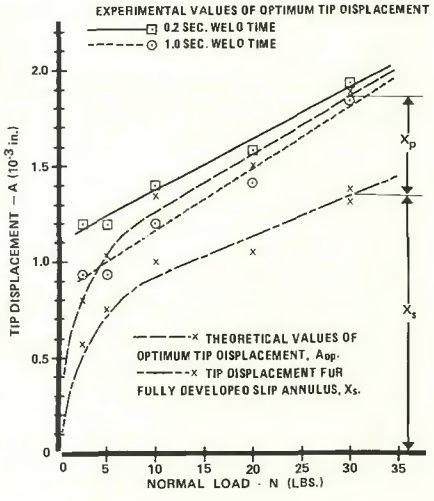

Fig. 14 — Theoretical and experimental values of the optimum sonotrode tip displacement for tensile weld strength (2024-T351 Al, in air)

The values of μ were calculated by using Eq. 13 and are plotted for different applied normal loads in Fig. 17. These values of μ were obtained by substituting X_s as listed in Table 1 into Eq. 13, and are found to be exceedingly high compared to the ordinary coefficient of friction for degreased 2024-T351 aluminum. Furthermore, the curve shows that μ is not a constant but a function of normal load N. An experimental equation of μ as a function of the normal load for 2024-T351 aluminum was obtained from the curve shown in Figure 17.

$$\mu = 10\,(N)^{-1/3} \qquad (16)$$

Another expression of X_s for 2024-T351 aluminum has been obtained by substituting Eq. 16 into Eq. 6.

$$X_s = 18.8\,(N/E^2 d)^{1/3} \qquad (6\text{-a})$$

From Eqs. 8, 6-a, and 10

$$A_{op} = [18.8\,(E^2 d)^{-1/3} + 0.44\gamma\,(d/E)^{1/3}]\,N^{1/3} \qquad (8\text{-a})$$

Eq. 8-a is verified by the calculated values of optimum amplitude as shown in Fig. 18.

$$A_{op} = 0.58\,N^{1/3} \qquad (8\text{-b})$$

Shear stresses developed at the final weld area by friction forces were calculated for the optimum welds and are shown in Table 3. Since the exact measurement of the final weld area is difficult, broken weld areas were used for the calculation, neglecting the work hardening effect. The calculation showed that the shear stresses developed at the final weld area by the friction force are fairly constant and are about 2.2 to 2.8 times higher than the shear yield strength of the material. These high shear stresses for the plastic deformation in the sublayer are due to the geometric constraints imposed by the surrounding material and the high strain rates developed during ultrasonic welding. The same geometric constraint can be found in the case of indenters pressed into flat material (Ref. 24). Similarly, the shear stresses calculated in Table 3 may well represent the stress required to plastically deform the constrained sublayer, and the original assumption that the sublayer enveloping the weld interface undergoes plastic deformation is justified.

The micrograph of an ultrasonic weld of OFHC copper in Fig. 19-b shows the lenticular shape of the sublayer plastic zone and both sublayer and peripheral cracks. An interesting phenomenon observed at the OFHC copper weld interface is the recrystallization occurring at the weld. Severely deformed sublayer partially self annealed to a fine grain structure is shown in Fig. 19-c, demonstrating that recrystallization is an auxiliary bonding mechanism for ultrasonically welded OFHC copper.

Many of the broken welds of 2024-T351 aluminum revealed grooves around the periphery at the leading and trailing edges of the weld as shown in Fig. 20. These grooves are attributed to the peripheral cracks already present after ultrasonic welding. The leading and trailing edges of the welds are most susceptible for peripheral cracks. The presence of peripheral cracks are shown clearly in Fig. 19-b for a sectioned specimen of ultrasonically welded OFHC copper. Some of the broken welds showed that gross sliding occurred at the weld, probably because of excessive electric power input combined with an insufficient normal load.

The tensile weld strength increases with increased normal load at high power range, but in the low

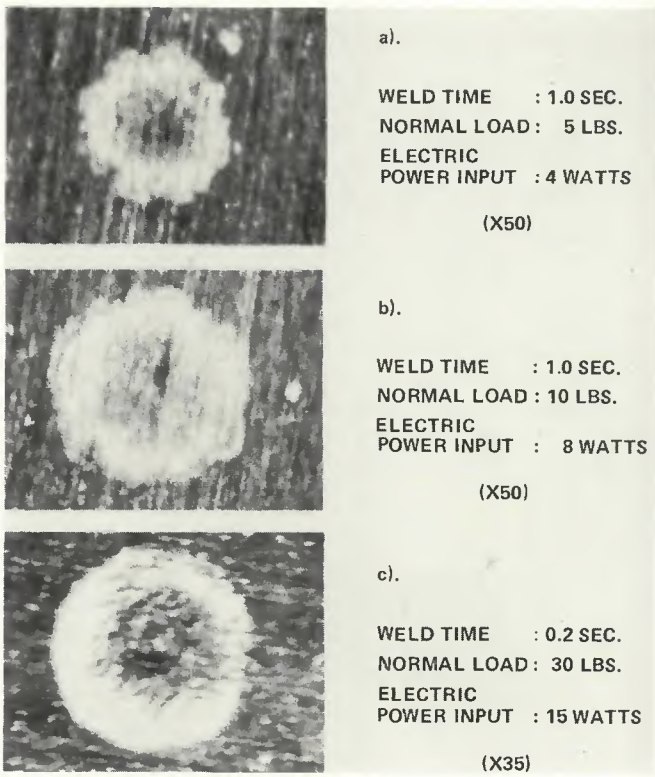

Fig. 15 — Micrographs of broken welds showing slip annuli (2024-T351 Al, in air)

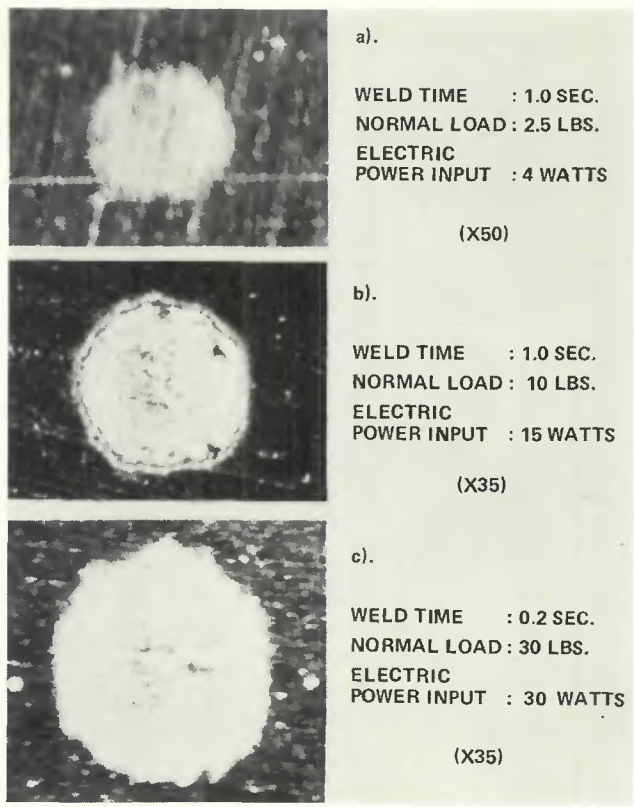

Fig. 16 — Micrographs of broken welds showing fully developed slip annuli (2024-T351 Al, in air)

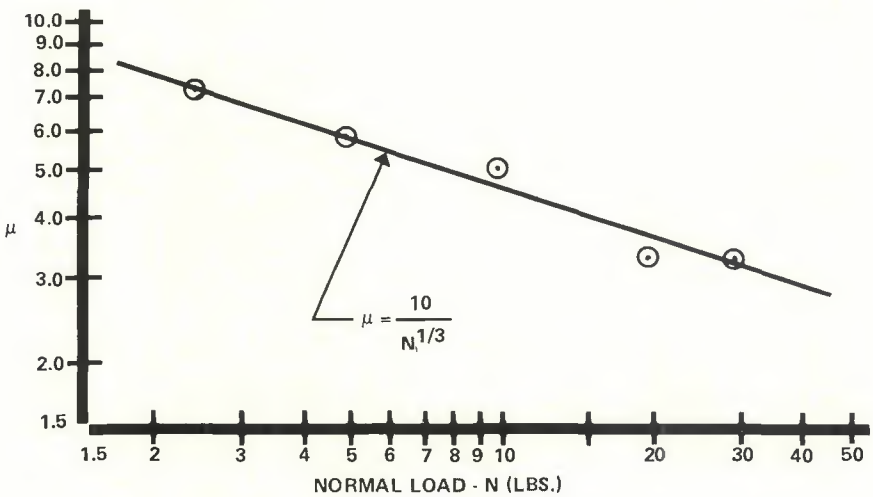

Fig. 17 — Coefficient of friction when an oscillating tangential vibration is applied (2024-T351 Al, in air)

Table 3 — Computed Shear Stresses by Friction Force Developed at Optimum Welds[a]

N, lb	μ [b]	Broken weld area, 10^{-4} in.^{2} t = 0.2 sec	Broken weld area, 10^{-4} in.^{2} t = 1.0 sec	Average broken weld area, 10^{-4} in.^{2}	$\tau = \frac{\mu N}{\text{weld area}}$, 10^3 psi
30	3.3	15.2	15.0	15.1	65.5
20	3.3	10.9	10.7	10.8	61.1
10	5.1	8.4	6.2	7.3	69.9
5	5.9	4.2	3.2	2.7	79.7
2.5	7.3	3.1	2.3	2.7	67.5

(a) Material: 2024-T351 aluminum; environment: air.
(b) See fig. 17.

power range it increases first, then decreases (Ref.21). High normal loads are detrimental to weld strength for low power welding, because correspondingly small amplitude of vibration cannot produce a fully developed slip annulus or proper plastic deformation at the weld interface.

The effect of weld time on tensile weld strength was checked for two different weld durations. The weld time of 0.2 sec gave higher tensile weld strength, than 1.0 sec weld time, but the time effect is less significant for higher normal loads. The establishment of an optimum weld time is important to increase the production rate of reliable products.

A vacuum environment of 2×10^{-7} to 4×10^{-7} torr does not provide a significant improvement in tensile weld strength for 2024-T351 aluminum with 5 lb normal load. However, higher tensile weld strengths were obtained in the same vacuum environment for 20 lb normal loads, especially when higher power inputs were used, as shown in Fig. 11-e. Also, the optimum power input moved from 45 W in air to 90 W in vacuum. In all vacuum tests the broken oxide particles, commonly found around the weld formed in air, were absent.

The changes in appearance of the broken weld are generally related to the electric power input and normal load used. As power increased from 2 to 140 W, the following order of changes was common. At low powers, a slip annulus was produced.

Then a fully developed slip annulus was observed, which grew to an elliptical weld area having shallow grooves around the periphery at the leading and trailing edges of the weld. These grooves grew deeper and sometimes metal slivers were extruded from the weld in the direction of ultrasonic vibration. After this stage, two different appearances were observed depending on the normal load used. Shiny sliding paths were shown for low normal loads (2.5 and 5 lb) and severely deformed irregular surfaces were produced for high normal loads.

To find the effect of increased power on the quality of a weld, the tensile breaking stresses (tensile weld strength divided by broken weld area) were plotted as a function of electric power input in Fig. 21. The result implies that the deterioration of weld quality is very sensitive to the power increase if a low normal load is used. Also, Fig. 21 indicates that the optimum tensile breaking stresses are constant.

To compare the shear strength of welds to the tensile strength, 2024-T351 aluminum and OFHC copper welds were fractured by shear. A normal load of 20 lb and a 1.0 sec weld time were used for both materials. The shear weld strengths of 2024-T351 aluminum showed a gradual increase until electric power input reached 75 W, then decreased slowly, as shown in Fig. 11-e. At low power levels, the tensile weld strengths were considerably higher than shear weld strengths, but at higher power ranges both strengths were approximately equal. This may be due to the fact that peripheral cracks do not grow deep enough and sublayer cracks are absent at a lower power level. At high power levels the extended cracks, especially sublayer cracks, may occur and decrease the effective weld area for tensile strength, as illustrated in Fig. 22. The shear strength, however, is not seriously affected by the presence of deeply grown peripheral cracks and sublayer cracks, since shear failure often develops along the weld interface.

The foregoing relationship is more clearly shown in Fig. 23 which includes tensile and shear strength curves for OFHC copper with 20 lb normal load and 1.0 sec weld time. Again, at a power range lower than 70 W tensile weld strengths were higher than shear weld strengths. However, at power levels larger than 70 W the shear weld strengths were higher than tensile weld strengths.

For OFHC copper, vacuum environment resulted in higher shear weld strengths than air environment, as shown in Fig. 23. Previous tests showed that tensile weld strengths were also improved by a vacuum environment for this material (Ref. 19).

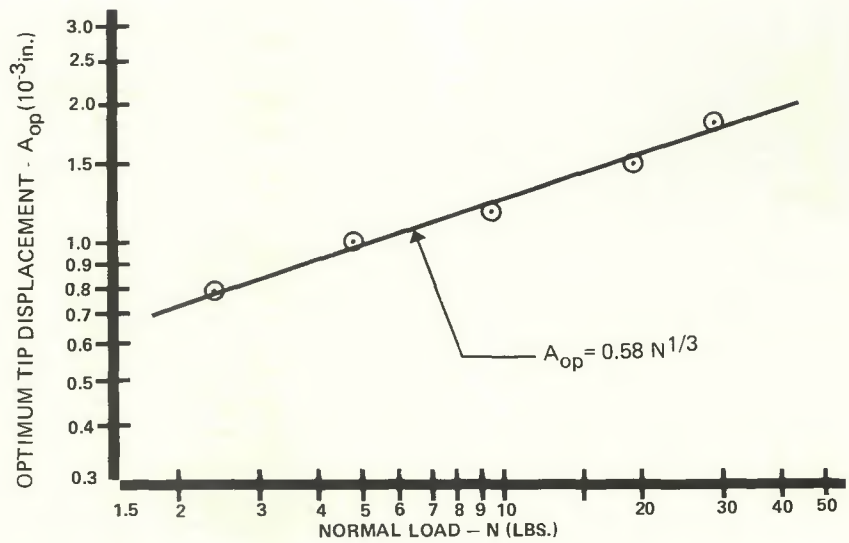

Fig. 18 — Theoretical values of the optimum sonotrode tip displacement (2024-T351 Al, in air)

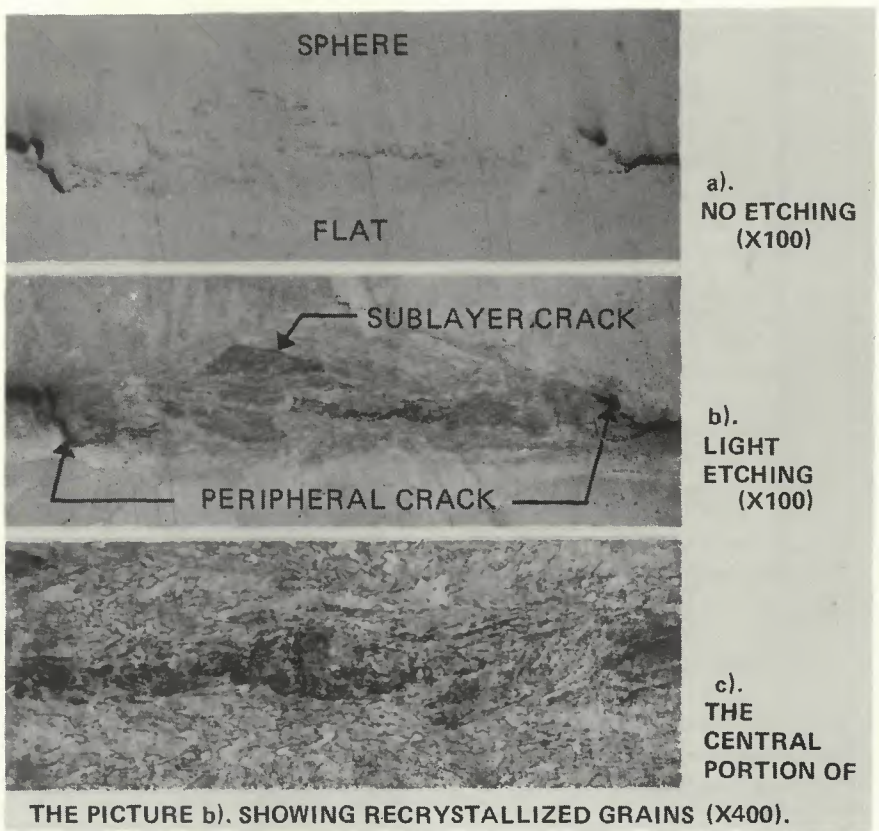

Fig. 19 — Sectioned view of a OFHC copper weld (not reduced). Normal load, 20 lb; weld time, 1.0 sec; power, 80 W; in air

The lack of oxidation in a vacuum environment helps metal-to-metal contact by not forming additional layers of oxides on the freshly exposed metal surfaces during slip and plastic deformation process. This is the most probable reason for higher weld strengths in a vacuum environment than in an air environment.

Conclusions

From this theoretical and experimental investigation for ultrasonic welding of 2024-T351 aluminum and OFHC copper under the described test conditions, the following conclusions are presented:

1. The mechanism of ultrasonic

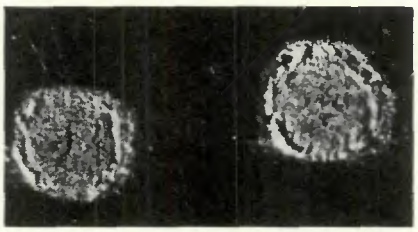

Fig. 20 — Broken welds of 2024-T351 aluminum after tensile test in air showing peripheral grooves. Normal load, 30 lb; weld time 0.2 sec; (left) 60 W; (right) 75 W. (X20, reduced 41%)

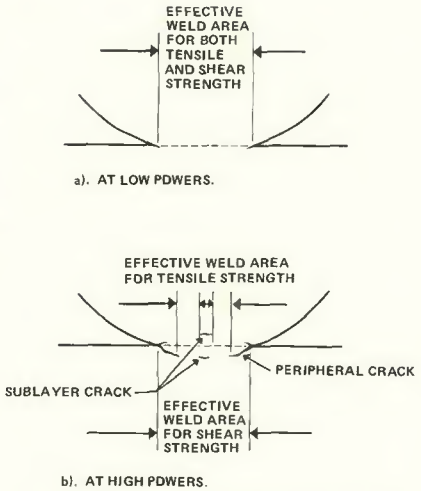

Fig. 22 — Effective weld area for tensile strength and shear strength of the weld

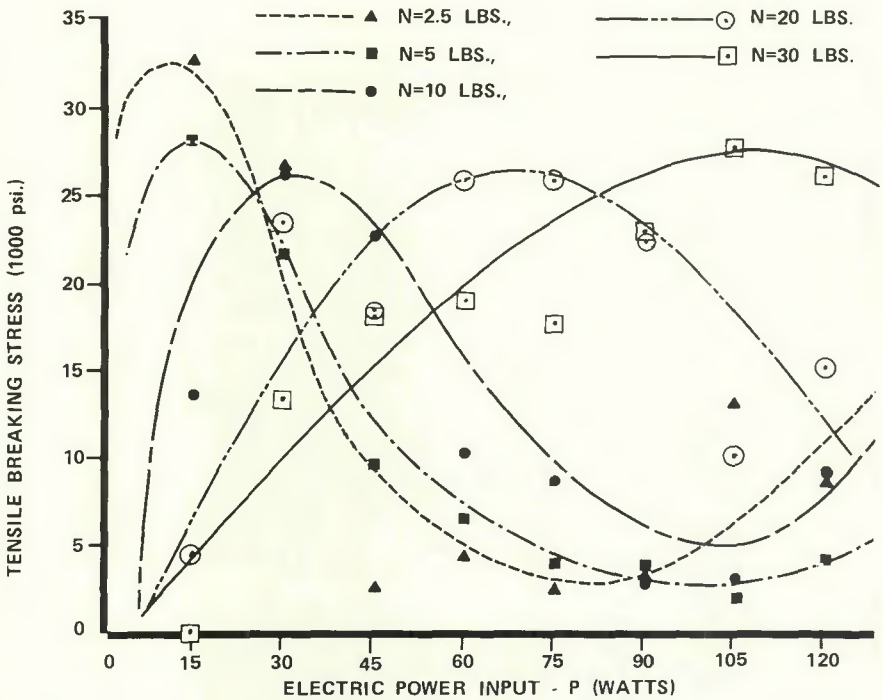

Fig. 21 — Tensile breaking stresses of 2024-T351 aluminum welds in air. Weld time, 0.2 sec

welding is basically solid state bonding such as adhesion, mechanical interlocking of the surfaces, recrystallization, and possibly diffusion.

2. Bonding is accomplished by two different processes, interfacial slip and sublayer plastic deformation. Both processes contribute to metal-to-metal contact.

3. Optimum welds are produced when the maximum slip area at the interface and proper plastic deformation in the sublayer are achieved. The relative displacement between two workpieces by ultrasonic vibration is important to achieve these conditions.

4. The optimum sonotrode tip displacement is the linear addition of the displacement necessary for a fully grown slip annulus and that for a proper sublayer plastic deformation.

5. For an optimum welding condition, a higher normal load requires a higher electric power input or a larger tip displacement.

6. Excessively high electric power input or large vibration amplitude deteriorates weld integrity by introducing sublayer and peripheral cracks.

7. The vibration amplitude or displacement at the sonotrode tip is a function of the electric power input for a particular ultrasonic welding system.

8. The shear stresses developed by friction force at the optimum welds are constant. The tensile breaking stresses of the optimum welds are also constant.

9. The values of coefficient of friction μ for 2024-T351 aluminum when an oscillating tangential vibration is applied at the contact between an elastic sphere and an elastic flat of the same material are higher than that of sliding friction and are a function of normal load.

10. A vacuum environment of 2×10^{-7} to 4×10^{-7} torr does not significantly improve the weld strength of 2024-T351 aluminum.

11. Due to the presence of sublayer cracks and peripheral cracks at high power levels, ultrasonic welds are more reliable for shear loads than tensile loads.

References

1. "Ultrasonic Welding," Chapter 49, Welding Handbook, 5th Edition. American Welding Society, Section III, "Welding, Cutting and Related Processes."

2. Daniels, H. P. C., "Ultrasonic Welding," *Ultrasonics,* October-December 1965, pp. 190-196.

3. Mindlin, R. D., Mason, W. P., Osmer, T. J., Deresiewicz, H., "Effects of an Oscillating Tangential Force on the Contact Surfaces of Elastic Spheres," Proceedings of the First National Congress on Applied Mechanics, 203, 1952.

4. Tylecote, R. F., *The Solid Phase Welding of Metals,* New York, St. Martin's Press, 1968.

5. Neppiras, E. A., "Ultrasonic Welding of Metals," *Ultrasonics,* July-September 1965, pp. 128-135.

6. Koenigsberger, F., Adair, J. R., *Welding Technology,* Third Edition, St. Martin's Press, New York 1966.

7. Jones, J. B., Maropis, N., et al, "Phenomenological Consideration in Ultrasonic Welding," *Welding Journal,* Vol. 40, July 1961, Res. Suppl., pp 289-s-305-s.

8. Ainbinder, S. B., "Certain Problems of Ultrasonic Welding," *Svarochnoe Proizvodstvo* (Welding Production), December 1959, Trans. by B.W.R.A.

9. Weare, N. E., Antonevich, J. N., Monroe, R. E., "Fundamental Studies of Ultrasonic Welding," *Welding Journal,* Vol. 30, August 1960, Res. Suppl., pp. 331-s-341-s.

10. Lewis, W. J., Antonevich, N. J., et al, "Fundamental Studies on the Mechanism of Ultrasonic Welding" Battelle Memorial Institute, December 1960, Wright Air Development Division.

11. Cl'shanskii, N. A., "On the Joining of Metals by Ultrasonic Welding," Moscow Institute of Energetics, *Avtomaticheskaya Svarka,* Volume 12, 1961, Trans. by Brutcher.

12. Weare, N. E., et al, "Research and Development of Procedures for Joining Similar and Dissimilar Heat-Resisting Alloys by Ultrasonic Welding," February 1959, WADC Tech. Rep. 58-479. Wright Air Development Center.

13. Bell, R. D., "Ultrasonic Seam Welding of Copper Sheet," Tech. Report, No. PRN-59, Princeton, November 4, 1962.

14. Timoshenko, S., *Theory of Elasticity.* First Edition 9th Impression, McGraw-Hill, 1934.

15. Mindlin, R. D., "Compliance of Elastic Bodies in Contact," *J. of Applied Mech.*, Volume 15, 1949, pp. 259.

16. Bowden, F. D., Tabor, D., *The Friction and Lubrication of Solids,* Oxford Univ. Press, 1950.
17. Shigley, J. E., *Mechanical Engineering Design,* McGraw-Hill Book Co., 1963.
18. Frisch, J., Chang, U., "Ultrasonic Welding of Metals in Vacuum," Final Report No. MD-69-2, August 1969.
19. Timoshenko, S., *Strength of Materials,* Part II, 2nd Edition, August 1941, pp. 350-356.
20. Pfaelzer, P. F., Frisch, J., "Ultrasonic Welding of Metals in Vacuum," Final Report No. MD-67-3, December 1967, University of California.
21. Frisch, J., Chang, U., "Optimal Strength of Ultrasonically Bonded Metals in Air and Vacuum," Final Report No. MD-70-2, September 1970.
22. *Aluminum Standards and Data,* The Aluminum Association, 2nd Edition, December 1969.
23. *Materials Engineering* — "Materials Selector Issue," Mid-Oct. 1966, Volume 64, No. 5. Reinhold Publishing Co.
24. Rabinowicz, E., *Friction and Wear of Materials,* John Wiley and Sons, Inc., N.Y. 1965.

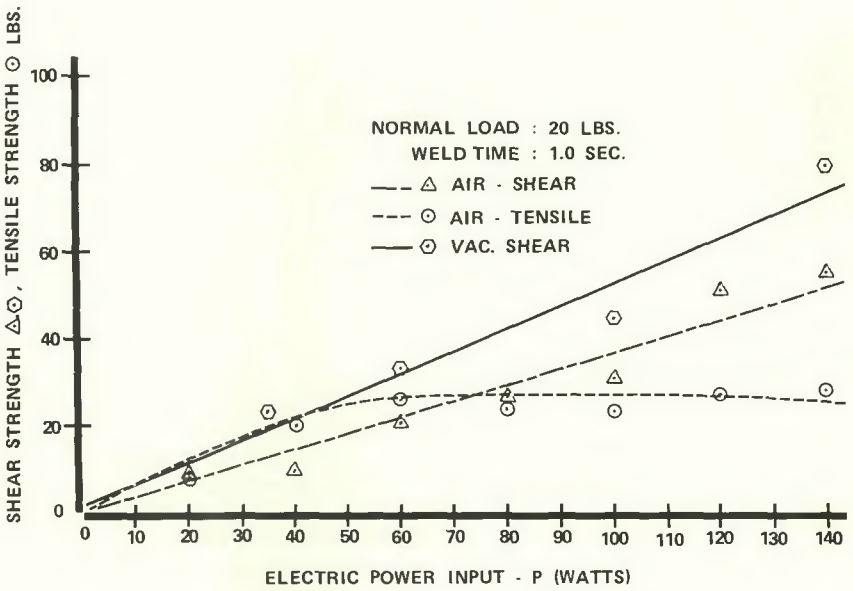

Fig. 23 — Shear strength and tensile strength of OFHC copper welds

STRUCTURAL WELDING CODE

Incorporates all of the welding requirements for the construction of buildings, bridges, and tubular structures.

Published in September, 1972, the Structural Welding Code, AWS D1.1-72, combines into a single document, completely updates, and replaces the Code for Welding in Building Construction, AWS D1.0-69, and Specifications for Welded Highway and Railway Bridges, AWS D2.0-69. Also, for the first time anywhere, requirements are presented for the design and fabrication of welded tubular structures.

These are the major changes affecting the building and bridge requirements which have been incorporated into the Code: (1) the addition of requirements for visual inspection for and repair of defects in cut edges of plates as received from the mill, (2) revision of weld quality and inspection requirements to remove ambiguity in previous editions relative to visual and nondestructive examinations, (3) increased tolerances on warp and tilt of girder flanges, and (4) inclusion of revisions issued in April of 1970*, including those to permit use of gas metal-arc (GMAW) and flux cored arc welding (FCAW) with prequalified procedures. Fatigue stresses for use in bridge design have been extended to include all steels used under the bridge portion of the Code.

To save time in the use of the Code, there is a complete index, an appendix containing selected definitions from Terms and Definitions, AWS A3.0-69, plus other welding terms used in the Code, and an appendix for conversions to the metric (SI) system. The Code is three-hole punched to permit insertion in binders if desired and to provide for the inclusion of revisions as issued. Its 8½ in. × 11 in. size is easier to read and use than the previous 6 in. × 9 in. editions of the Building Code and Bridge Specifications.

CONTENTS

The price** of the Structural Welding Code is as follows: sustaining member — $12.00; member — $12.00; associate member — $13.60; student member — $13.60; bookstores, public libraries, and schools — $12.80; and non-member (of AWS) — $16.00.

Send your orders for copies to the American Welding Society, 2501 N.W. 7th Street, Miami, FL 33125.

**April 1970 issue of Welding Journal, pp. 263-272.*

***Prices shown include 4th class postal delivery within the United States. For other than 4th class or to foreign countries, postage will be charged accordingly. Add 4% sales tax for orders to be delivered within the State of Florida. A handling charge will be added if payment does not accompany order.*